Science Translational Medicine
AAAS

www.sciencetranslationalmedicine.org/cgi/content/full/8/367/367ra167/DC1

Supplementary Materials for

Internalization of secreted antigen–targeted antibodies by the neonatal Fc receptor for precision imaging of the androgen receptor axis

Daniel L. J. Thorek, Philip A. Watson, Sang-Gyu Lee, Anson T. Ku, Stylianos Bournazos, Katharina Braun, Kwanghee Kim, Kjell Sjöström, Michael G. Doran, Urpo Lamminmäki, Elmer Santos, Darren Veach, Mesruh Turkekul, Emily Casey, Jason S. Lewis, Diane S. Abou, Marise R. H. van Voss, Peter T. Scardino, Sven-Erik Strand, Mary L. Alpaugh, Howard I. Scher, Hans Lilja,* Steven M. Larson,* David Ulmert*

*Corresponding author. Email: ulmerth@mskcc.org (D.U.); liljah@mskcc.org (H.L.); larsons@mskcc.org (S.M.L.)

Published 30 November 2016, *Sci. Transl. Med.* **8**, 367ra167 (2016)
DOI: 10.1126/scitranslmed.aaf2335

The PDF file includes:

Other Supplementary Material for this manuscript includes the following:
(available at www.sciencetranslationalmedicine.org/cgi/content/full/8/367/367ra167/DC1)

Video S1 (.mp4 format). Confocal z-stack through prostate gland of genetically engineered hK2-expressing mouse.

Supplementary Materials:

Materials and Methods:

Expression and purification of hu11B6

HEK293 cells were expanded to a cell density of 1×10^6 cells/mL in a 2 L suspension culture in FreeStyle 293 Expression Medium (Life Technologies). The plasmid DNA (expression vectors p11B6VLhV1hk and p11B6VHhV1hIgG$_1$) containing the nucleotide sequences for the heavy and light chains of hu11B6 IgG1/k was then mixed with the transfection agent and incubated for 10 min at room temperature (RT). The DNA transfection agent mix was slowly added to the cell culture while slowly swirling the flask. The transfected cell culture was then incubated at 37 °C with 8% CO_2 on an orbital shaker platform rotating at about 135 rpm for seven days. Culture medium was harvested by centrifugation and filtered through 5 μm, 0.6 μm, and 0.22 μm filter systems. Antibodies were purified by Protein G chromatography, and the buffer was changed to PBS pH 7.4 by dialysis; subsequently, the antibodies were concentrated by ultrafiltration. Concentration was measured by absorbance. Overall yield was 13.1 mg (~6.5 mg/L).

Tissue histology and autoradiography

After mice were euthanized, a tissue package containing prostate lobes, seminal vesicles, and prostatic urethra was surgically excised and incubated in Tissue-Tek optimal cutting temperature compound (Sakura Finetek USA, Inc.) on ice for 45 minutes, and then snap-frozen on dry ice in a cryomold. Sets of contiguous 15 or 100 μm-thick tissue sections were cut with a CM1950 cryostat microtome (Leica Microsystems Inc.) and arrayed onto SuperfrostPlus glass microscope slides. Sections stained for actin and DNA (100 μm sections) were incubated with 200 μL of 10 U/mL rhodamine-phalloidin (Life Sciences Inc.) in PBS for 2-3 hours at RT in a covered container to prevent evaporation, and then washed with PBS twice. DNA/nuclei staining was performed by incubating the slides for 10 min in 5 μg/mL DAPI in PBS, followed by a wash with PBS. Slides were then air-dried, and a drop of Mowiol A-48 (Calbiochem Inc.) was placed on the slide before adding a mounting cover glass. Slides were then stored at –20 °C. Immunostaining for AR was performed by incubating

slides with blocking solution (2% BSA in PBS) for 15 min at room temperature and staining with 1:200 dilution of anti-AR polyclonal antibody (NH27) for 45 min followed by Texas red-conjugated goat anti-rabbit antibody (ICN) for 45 min at room temperature. Stained slides were then washed and mounted.

Sections intended for autoradiography were fixed in 4% paraformaldehyde solution in phosphate-buffered saline (Affymetrix) for 5 minutes, washed twice, air-dried, and stained with hematoxylin and eosin (H&E). The immunohistochemical detection of Ki-67, AR (N-20), and c-MYC was performed at the Molecular Cytology Core Facility of Memorial Sloan Kettering Cancer Center using a Discovery XT processor (Ventana Medical Systems). Before staining, all sections were blocked for 30 minutes in 10% normal goat serum with 2% BSA in PBS. Sections stained for Ki-67 were incubated with 0.4 µg/mL of the primary antibody (rabbit polyclonal Ki-67 antibody; Vector Labs, cat.#: VP-K451) for 2 hours, followed by a 30-minute incubation with biotinylated goat anti-rabbit IgG (Vector Labs, cat.#:PK6101) at 1:200 dilution. Sections stained for AR (N-20) were incubated for 3 hours with a polyclonal rabbit antibody (Santa Cruz, cat.#: SC-816) at 1 µg/ml concentration, followed by 16 minutes of incubation with biotinylated goat anti-rabbit IgG (Vector labs, cat#:PK6101) at 1:200 dilution. c-MYC staining was performed by incubating sections for 5 hours with a primary anti-c-MYC antibody (N terminal, rabbit polyclonal, Epitomics, cat.#: P01106), followed by 60 minutes of incubation with biotinylated goat anti-rabbit IgG (Vector Labs, cat.#: PK6101) at 1:200 dilution. Blocker D, streptavidin- HRP, and DAB detection kit (Ventana Medical Systems) were used according to the manufacturer's instructions. Stained tissue sections were placed in a film cassette against a Fuji film BAS-MS2325 imaging plate (Fuji Photo Film Co.) to acquire digital autoradiograms. The slides were exposed for 48 hours, approximately 168 hours after injection of ^{89}Zr-DFO-11B6. Exposed phosphor plates were read by a Fujifilm BAS-1800II bio-imaging analyzer (Fuji Photo Film Co.), generating digital images with 50 µm pixel resolution. Digital images were obtained with an Olympus BX60 System Microscope (Olympus America, Inc.) equipped with a motorized stage (Prior Scientific, Inc.). Subsequently, H&E images were acquired to the same resolution as the DAR data. DAR images were manually aligned to the H&E images using rigid planar transforms.

Transgenic KLK2 mouse models

Site-directed mutagenesis of APLILSR to APLRTKR at positions 4, -3, and -2 the zymogen sequence of *KLK2* was performed using a Quick Change Lightning Mutagenesis Kit (Stratagene). This enabled furin, a ubiquitously expressed protease in rodent prostate tissue, to efficiently cleave the short activation peptide at the cleavage site (–1 Arg/+1 Ile), resulting in functional hK2. Sequencing was performed to verify the genotype using the following primers: 5'-TTC TCT AGG CGC CGG AAT TA-3' (forward), 3'-CCC GGT AGA ATT CGT TAA CCT-3' (reverse). A transgenic mouse model was established by cloning the described construct into a SV40 T-antigen cassette downstream of the short rat probasin promoter (pb). This construct was microinjected into fertilized mouse embryos (C57BL/6) and implanted into pseudopregnant female mice. A cancer-susceptible transgenic mouse model with prostate specific hK2 expression was created by crossing the pb_*KLK2* transgenic model with the Hi-MYC model (ARR2PB-Flag-*MYC*-PAI transgene). A schematic of the strategies used is included as figure S25. Integration of genes into the genome of the offspring was confirmed by Southern blot analysis and PCR (fig. S26). Mice were monitored closely in accordance with IACUC-established guidelines and RARC animal protocol (# 04-01-002).

Castration- and enzalutamide-resistant liver metastasis model

Previously surgically castrated mice with a body weight of 28–30 g were anesthetized by intraperitoneal injection of ketamine (75 mg/kg) and xylazine 2% (15 mg/kg). Anesthetized animals were placed in a supine position, draped, and prepared for sterile surgery. A 10 mm midline incision was made on the upper abdomen through the skin and peritoneum. The left lobe of the liver was separated from the caudate and median lobe, and was exposed and immobilized. A Hamilton syringe with a 26-gauge needle was used for injection of a 10 µL mixture of LREX' tumor cells (10^5 cells) and Matrigel (1:1). The puncture site was closed by gentle pressure for approximately 1 min with a moistened cotton-tipped applicator stick. After tumor cell inoculation, the liver lobe was repositioned anatomically. The abdominal wall was then closed in a two-layer technique with a resorbable suture for the fascia and subcutaneous tissue (5/0 vicryl, Ethicon) and a nonresorbable suture for the

skin (5/0 prolene, Ethicon). A 0.05 mg dexamethasone pellet (60 day release) was subcutaneously implanted at the end of the procedure to confer enzalutamide resistance and activate the glutocorticoid receptor (*47*). Animals received postoperative analgesia by subcutaneous injection of carprofen (5 mg/kg) once daily for 3 days after surgery. Daily enzalutamide (10 mg/kg) treatment was given by gavage. Tumor development was followed with bioluminescence imaging and confirmed with MR imaging.

Antibody humanization

The acceptor framework used for the grafting was derived from the human immunoglobulin germline genes showing the highest sequence similarity with the variable domains of the parental 11B6 antibody. The genes were identified by comparing the amino acid sequences of the mouse 11B6 variable light (V_L) and heavy (V_H) domains to the human immunoglobulin germline sequences in NCBI database. The germline V gene IGKV4-1*01 (GenBank: Z00023.1) together with the short IGKJ2 gene (GenBank: J00242.1) were selected to construct the V_L acceptor framework into which we grafted the CDRs of mouse 11B6 light chain. For the V_H acceptor framework, the V gene IGHV4-28*01 (GenBank: X05714.1) and J gene IGHJ1 (GenBank: AAB59411.1) were used. A 3D homology model of the mouse 11B6 was built to facilitate the evaluation of the influence of non-CDR residues on the CDR loop conformations. On the basis of the published data and visual inspection of the model, the following residues were adopted from the parental mouse 11B6: Leu4 in the light chain and Asn27, Thr30, Arg71, and Thr94 in the heavy chain. On the basis of structural analysis, certain CDR residues were obtained from the sequences of the human acceptor framework: an arginine was introduced in the position 54 in CDR-L2 to allow the formation of a salt bridge with another light chain residue Asp60, whereas Lys24 in CDR-L1 and Asn60 in CDR-H2 were included to maximize the content of human gene-derived amino acids in hu11B6, although they were predicted not to play a major role in antigen binding.

Codon optimized nucleotide sequences encoding hu11B6 variable heavy or light chains were designed, purchased as synthetic genes, and subcloned to obtain the mammalian expression vectors p11B6VLhV1hk (4300 bp) and p11B6VHhV1hIgG$_1$ (4900 bp) for the production humanIgG$_1$/kappa antibody.

11B6 immunohistochemistry

The murine 11B6 antibody was used on human tissue microarrays. Human tissue microarrays (US Biomax) included fine needle biopsies of normal prostate, primary adenocarcinoma, and metastatic foci. Four-µm sections were deparrafinized in xylene and rehydrated in decreasing ethanol dilutions. Endogenous peroxidase was blocked with 3% hydrogen peroxide buffer for 10 minutes. Antigen retrieval was performed by boiling in EDTA buffer (pH 9.0) for 20 min. Slides were subsequently incubated overnight in a humidified chamber with murine anti-hK2 (m11B6) at a 1:1000 dilution in 0.5% BSA/TBST followed by one hour incubation with Poly-HRP-anti-mouse/rabbit/rat IgG (Brightvision, Immunologic). The slides were developed with diaminobenzidine and lightly counterstained with hematoxylin and mounted.

FcRn affinity measurements

To test the effect of the H435A-11B6 antibody, which contains a point mutation (and the original 11B6 construct), we performed surface plasmon resonance (SPR) on a CM5 chip using a Biacore 3000 instrument. The chip and all reagents were purchased from GE Healthcare; experiments were conducted in assay buffer (67 mM phosphate buffer, 0.15 M NaCl, 0.05% Tween-20) adjusted to either pH 6.0 or pH 7.4. At the lower pH, FcRn has the ability to bind to the Fc portion of intact immunoglobulins (IgG_1), but at the higher pH this affinity drops to enable release of the antibody (*24*). Human FcRn (hFcRn) was bound to the chip by following the manufacturer's guidelines, with carbodiimide (EDC) and N-hydroxysuccinimide (NHS) in reaction buffer (10 mM sodium acetate, pH 5.0) and washed after immobilization with running buffer. Channels were blocked by ethanolamine after activation and immobilization and EDC and NHS washed off. The affinity of each antibody for the FcRn was evaluated with a flow rate of 30 µL/min at a concentration of 50 nM in each buffer condition. If binding was observed, association and dissociation rates were measured using the bivalent fitting model (BIAevaluation Software, Biacore).

Characterization of h11B6 affinity

After optimizing the experimental conditions, multiple binding measurements were performed for m11B6, hu11B6, DFO-hu11B6, and the antigen. From the collected data, the association and dissociation rate constants (k_{on} and k_{off}) and the dissociation constants (K_D) were calculated.

Supplementary Figures:

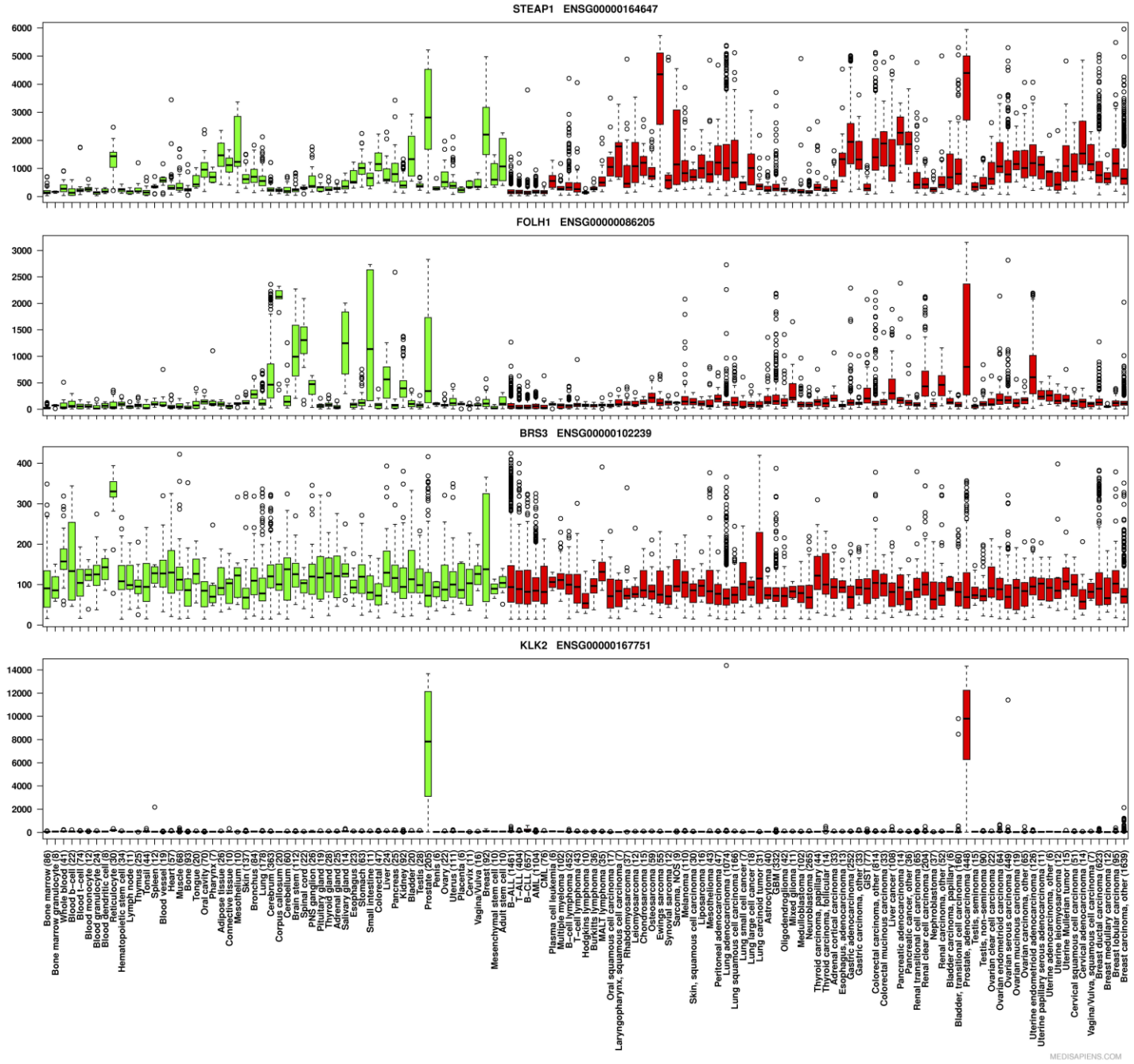

Supplementary Figure 1. Anatomical and disease-specific gene expression of candidate targets. Targeted agents for disease identification, characterization, and therapy include (A) six transmembrane epithelial antigen of the prostate 1 (*STEAP1*), (B) prostate-specific membrane antigen (*FOLH1*), and (C) GCPR bombesin receptor (*BSR3*). (D) AR-activity regulated human kallikrein-related peptidase 2 (*KLK2*) is restricted to the prostate and prostate-derived tissue, as well as adenocarcinoma of the breast under sex-steroid stimulation. Median expression is shown as a horizontal line, with 25 and 75 percentiles as lower and upper bounds of the boxes, with whiskers and outlier points extending to cover the remaining data. Data from the In Silico Transcriptomics Online database (*51*), an integrated human gene expression catalog of 60 healthy tissues (green), 104 malignant, and 64 other disease types (red).

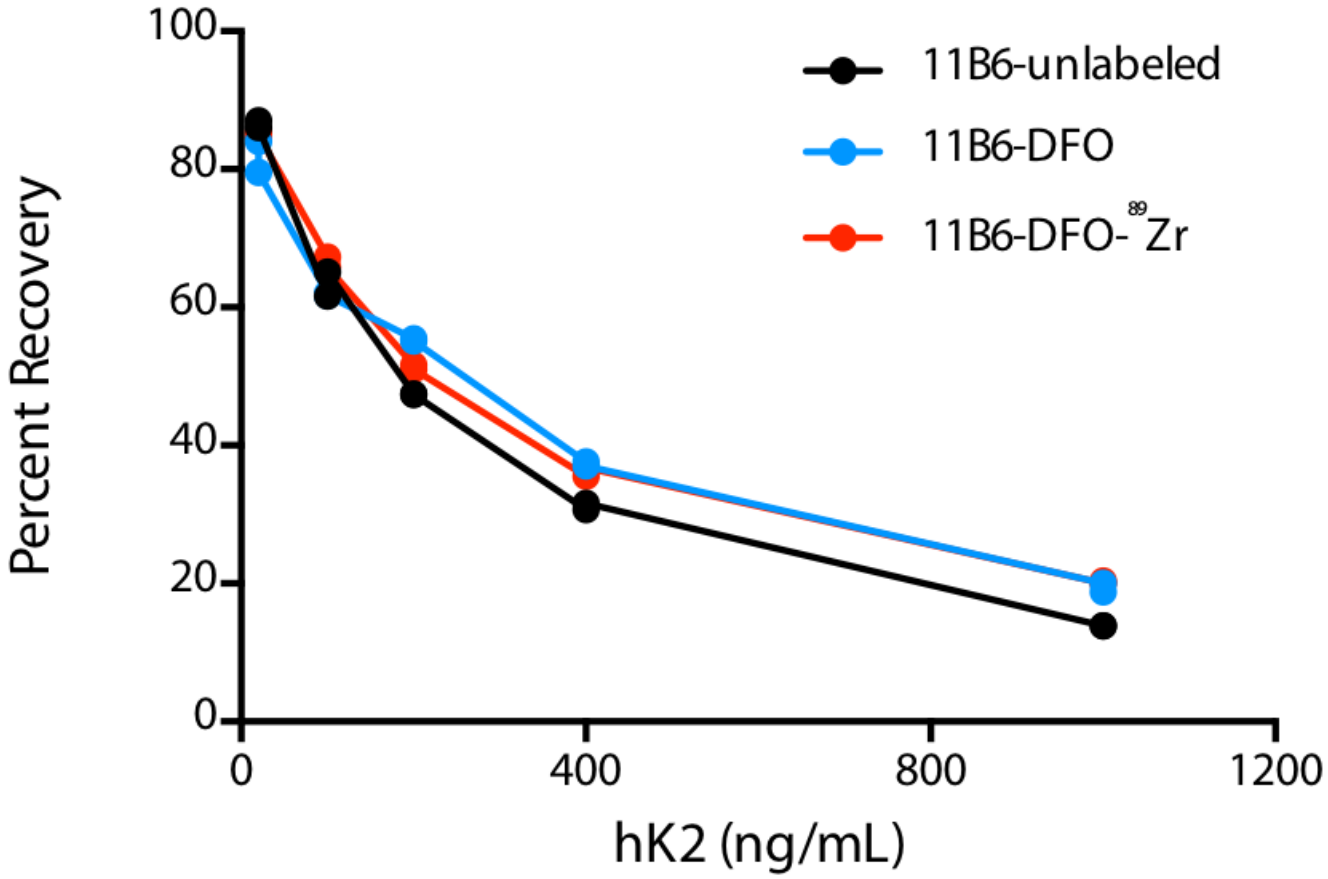

Supplementary Figure 2. Competition assay. Competition assay comparing the affinity of unlabeled 11B6 (black) to DFO-conjugated (blue), as well as ^{89}Zr-labeled DFO-11B6 (red). No significant differences in capture efficacy of free hK2 are noted for the conjugated or radiolabeled constructs.

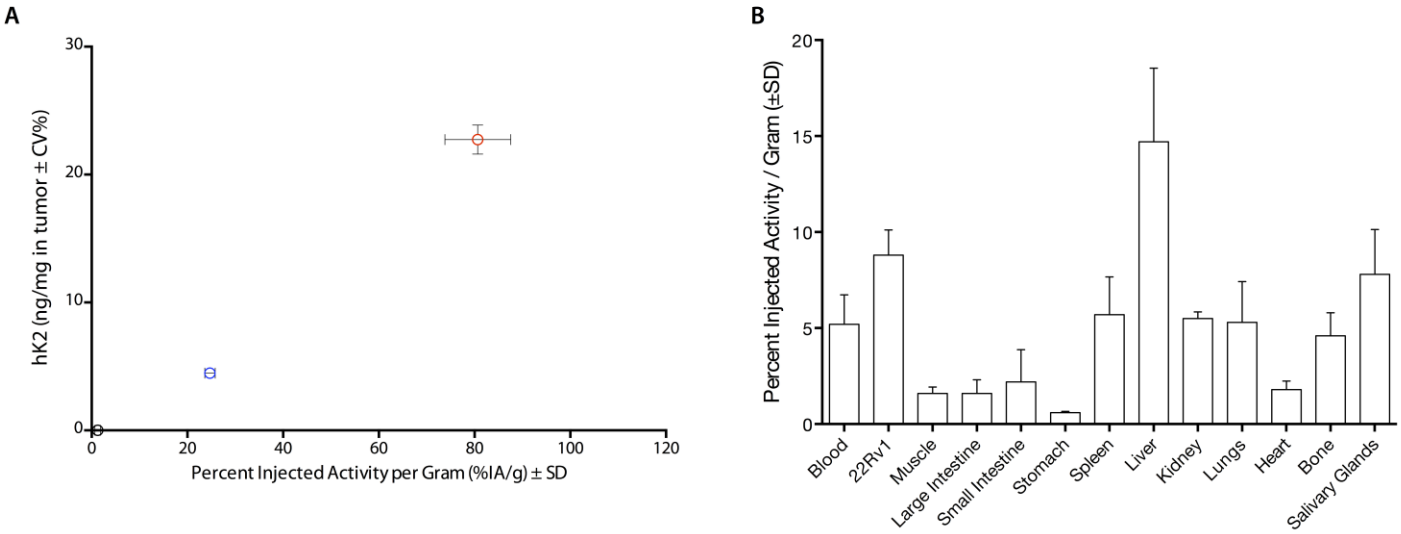

Supplementary Figure 3. ^{89}Zr-DFO-11B6 uptake and hK2 expression. (A) Protein expression and uptake of the tracer were correlated. Percent injected activity values were assessed by gamma-counting, and hK2 from lysate was measured by time-resolved immunofluorometric assay. hK2 protein values are expressed as ng per mg of total protein. (B) To evaluate the uptake of the tracer in a model of patients who have failed hormone therapy, we implanted 22Rv1 xenografts into the flank of castrated Balb/c nu/nu mice. Biodistribution demonstrates uptake at the tumor, consistent with the continued AR-driven hK2 expression.

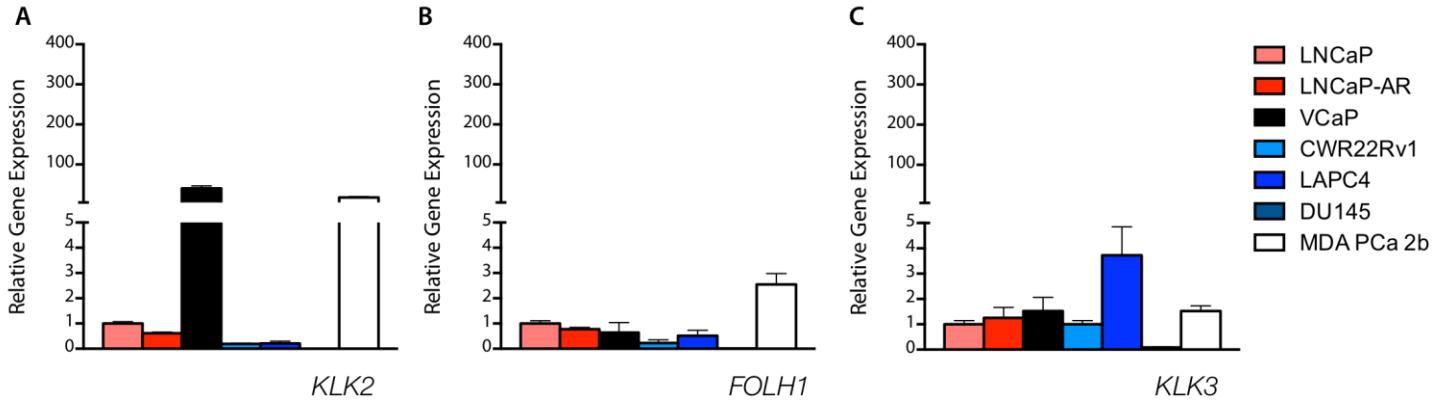

Supplementary Figure 4. Relative expression of putative prostate markers in PCa cell lines. RT-PCR was performed on 7 commonly used prostate cancer cell lines for genes of interest which included (A) *KLK2* (encoding hK2), (B) *FOLH1* (encoding PSMA, prostate-specific membrane antigen), and (C) *KLK3* (encoding PSA).

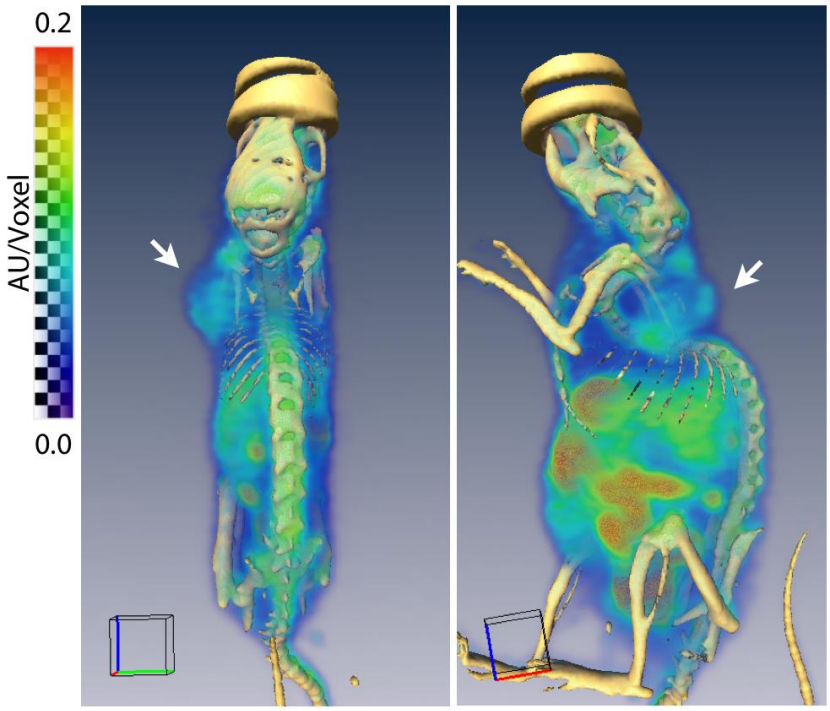

Supplementary Figure 5. ^{18}F-FDHT imaging. The distribution of ^{18}F-FDHT at 1.5 h after administration in a representative VCaP (arrow) bearing mouse. ^{18}F-FDHT is a radiolabeled analog of the non-aromatizable dihydrotestosterone. Tumor site indicated by arrow.

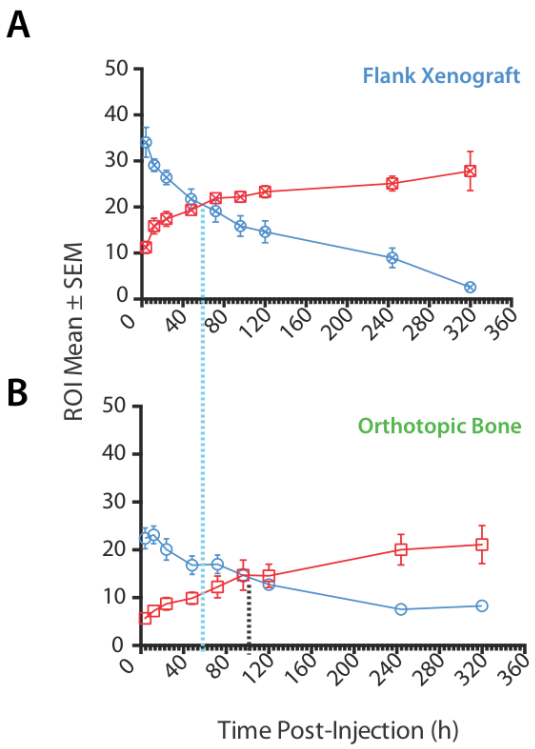

Supplementary Figure 6. Time-activity curves of LNCaP-AR subcutaneous and orthotopic xenografts. (A) The kinetics of uptake measured as %IA/g in the flank xenograft model are faster than in (B) an orthotopic bone model. Time-activity curves were plotted noninvasively from dynamic PET acquisitions at the times indicated and show tumor (red) and blood (blue) values. Blood values were assessed from the mean %IA/g of volumes of interest defined around the heart from PET datasets.

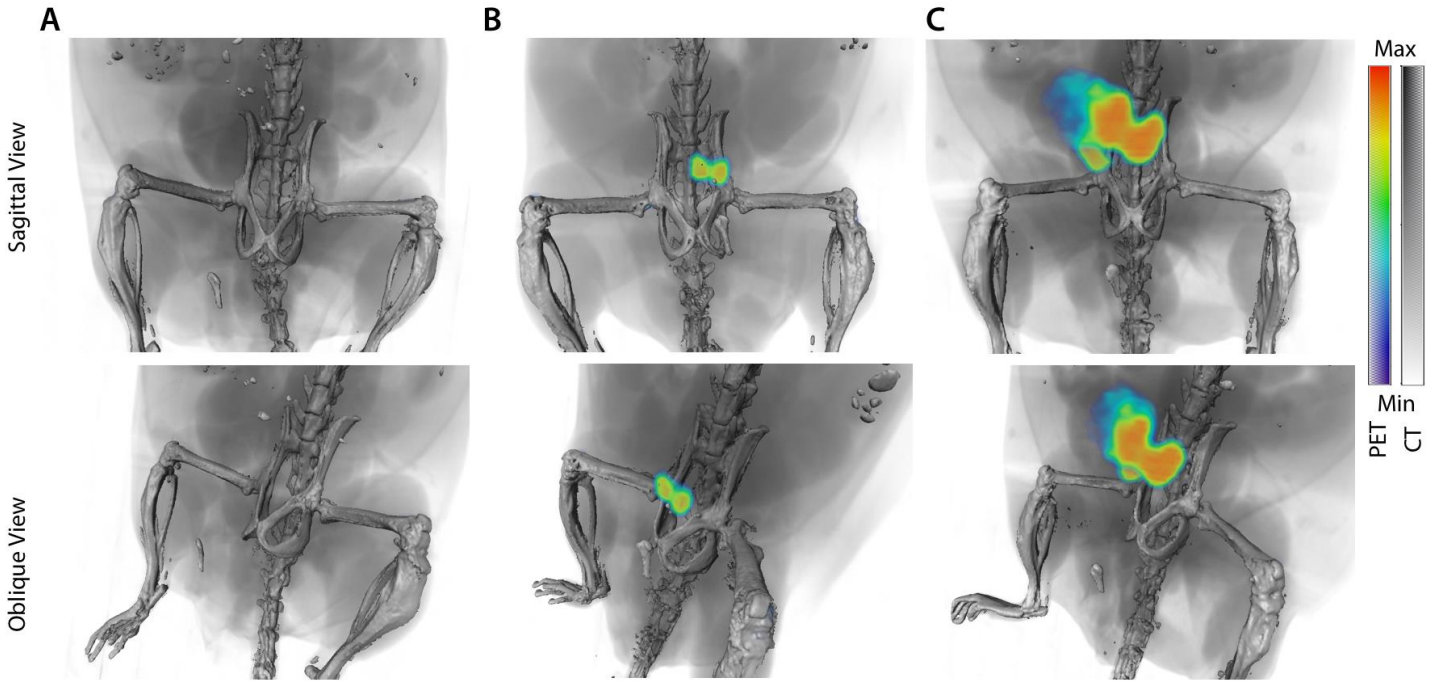

Supplementary Figure 7. ^{89}Zr-DFO-11B6 prostate and hK2-specific imaging in transgenic healthy and diseased mice. Sagittal and oblique views of three-dimensional ^{89}Zr-11B6 (50 µg) PET/CT fusion volumes of the pelvis in representative mice, with surface-rendered skeleton, 96 h after administration. (A) No uptake of the radiotracer is seen in a wild-type C57Bl/6 mouse (42 weeks). (B) Representative image of a mouse (51 weeks) that has been engineered to express the active hK2 protein under a prostate-specific promoter. At tracer dose, the 11B6 imaging agent is able to define the two ventral lobes (which express the most protein). (C) Crossing these transgenic animals with established models of prostate cancer, for example this representative hK2 X Hi-Myc mouse, yields greater uptake of the tracer in the cancerous prostate. Note that intact antibodies are excreted primarily through the liver, and therefore bladder signal is not seen.

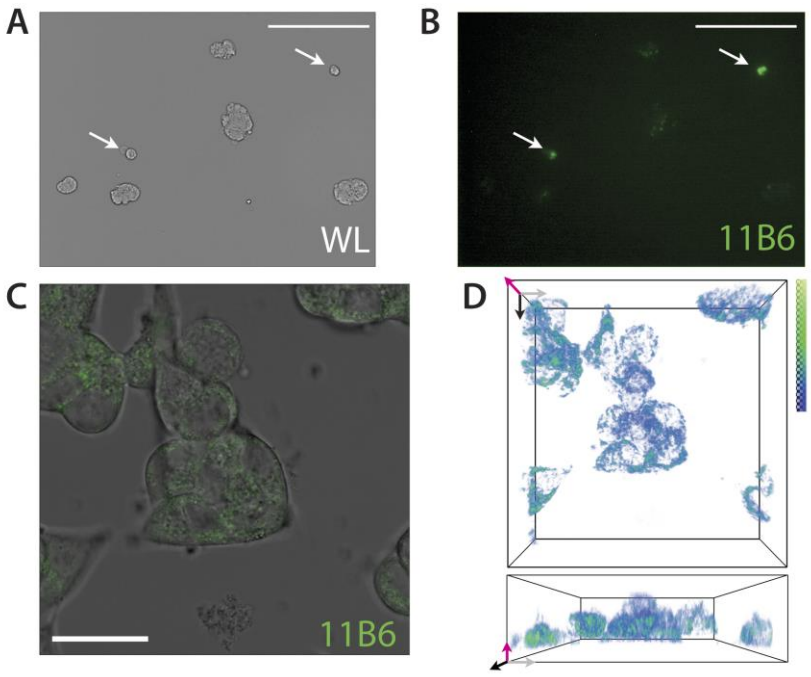

Supplementary Figure 8. Cy5.5-11B6 cellular uptake. (A) White light and (B) fluorescence imaging of a single cell suspension of hK2-expressing mouse prostate after intravenously administered Cy5.5-11B6 (scale, 120 µm). (C) Confocal microscopy of cultured VCaP cells incubated with Cy5.5-11B6 overlaid on differential interference contrast light image of cells (scale, 22 µm). (D) Three dimensional rendering of fluorescence distribution within the cells in XY (top) and YZ (bottom) perspectives.

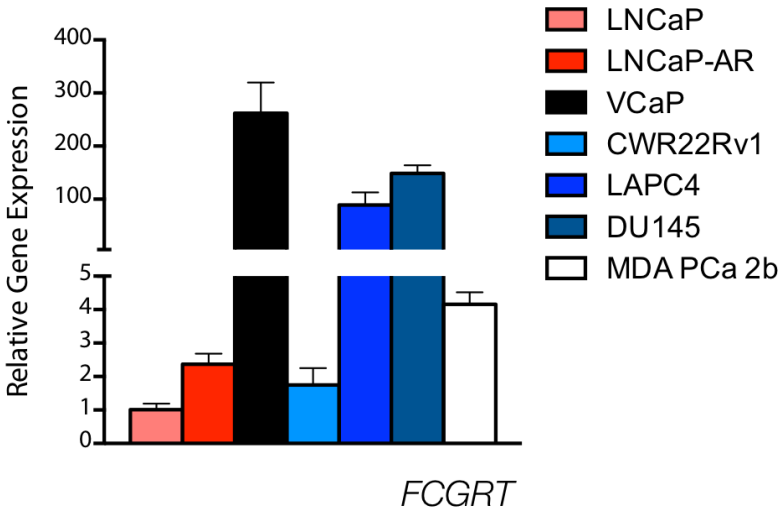

Supplementary Figure 9. FcRn gene expression. The expression of *FGCRT*, encoding the IgG-binding neonatal Fc receptor, across a panel of prostate cancer cell lines.

A

FcRn K_D (M)	pH 6.0	pH 7.4
11B6	2.6 ± 10^{-7}	no binding
H435A-11B6	no binding	no binding

B

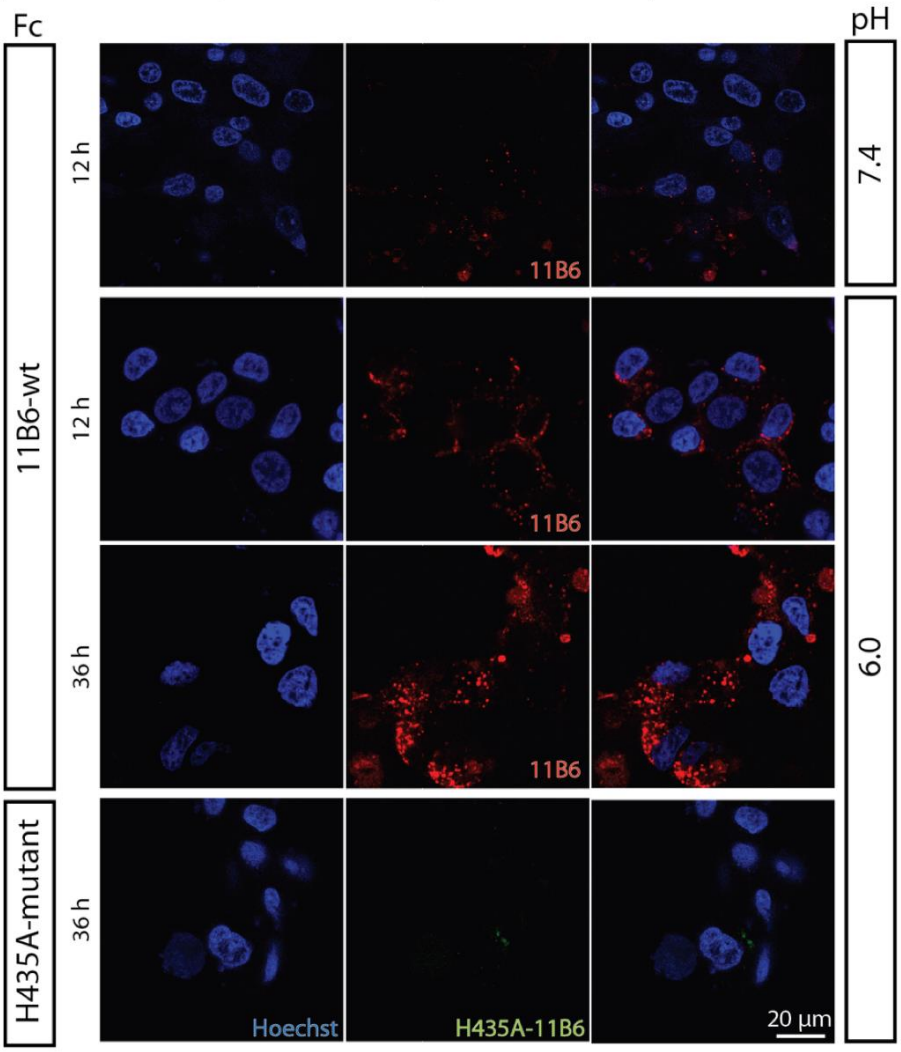

Supplementary Figure 10. FcRn-specific transport. (A) SPR determined dissociation constants for FcRn for 11B6 and H435A-11B6 at pH 6 and 7.4. (B) Exploiting the receptor's pH-dependent affinity, FcRn-mediated uptake is confirmed by increased uptake kinetics at low extracellular pH. Uptake is abrogated with H435A-modified 11B6.

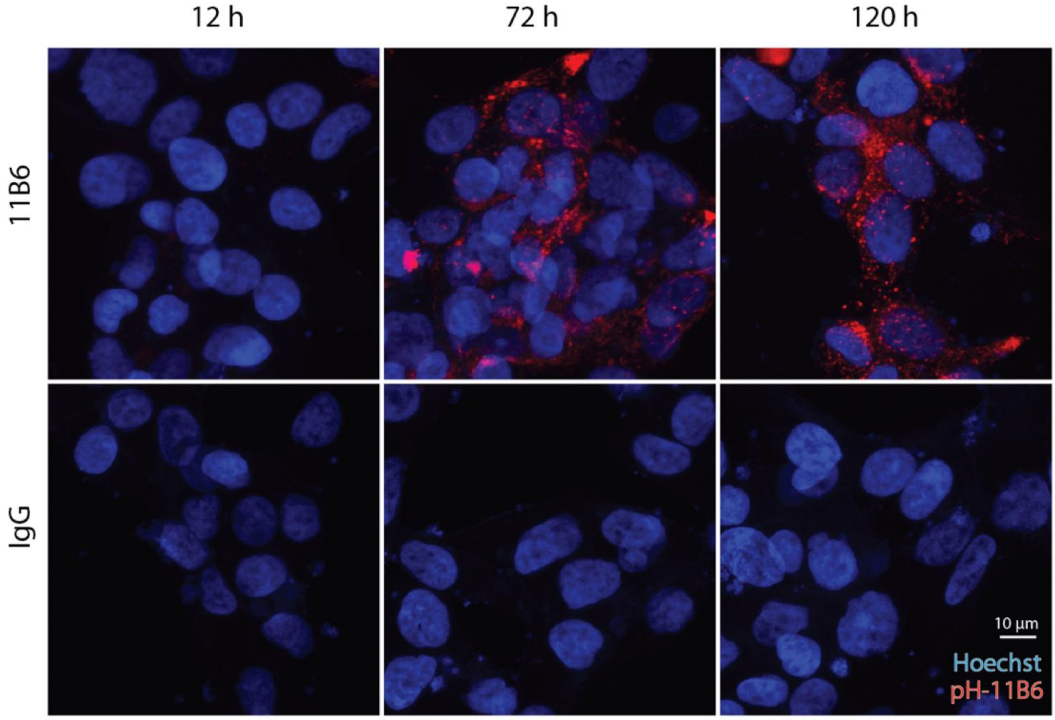

Supplementary Figure 11. Uptake of pH-responsive dye-labeled 11B6. Top row: 11B6, bottom row: control IgG. Prostate cancer cells (LNCaP) were pulsed with pH indicator dye-labeled antibody. Internalized 11B6 is not in an acidic environment at 12 h (but has been internalized; Figure 3). Fluorescence intensity increased in the acidic late endosomes at later time points. Control IgG was not detected.

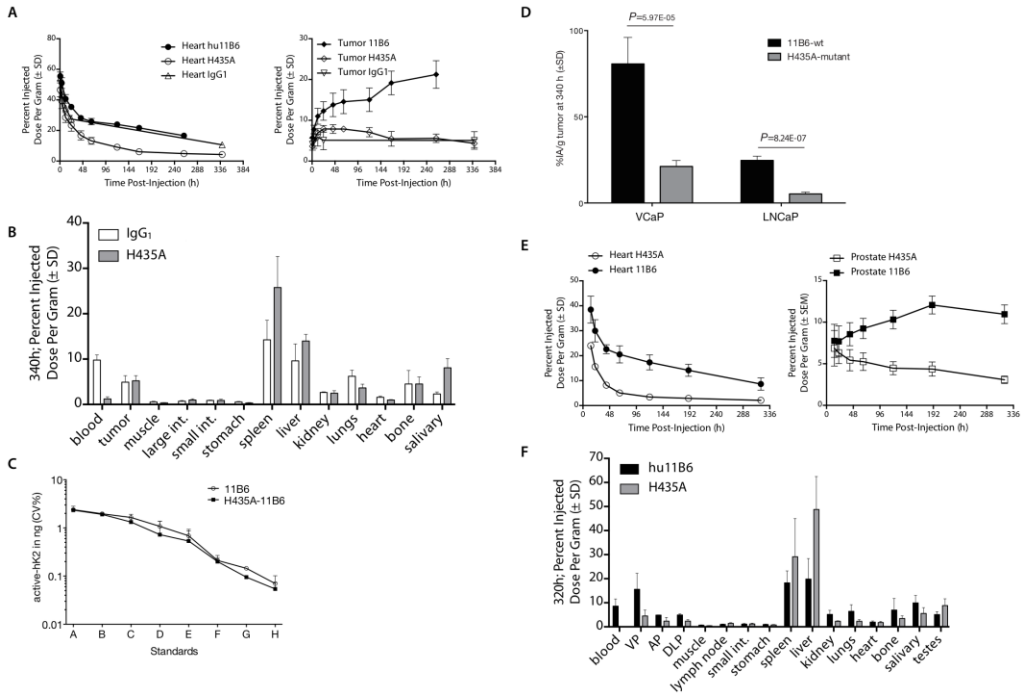

Supplementary Figure 12. Investigation of FcRn-mediated uptake of 11B6 complexed with hK2. (A) The comparison of uptake in LNCaP xenografts (and blood clearance from heart measurements) of the 11B6 antibody and the single point mutated H435A-11B6. (B) Ex vivo biodistribution of the two non-accumulating constructs (non-specific IgG1 and H435A) demonstrates the requirement for both hK2 binding and FcRn internalization. (C) In vitro verification of binding of both 11B6 and the H435A mutant to hK2 by immunofluorimetric competition assay. (D) Validation of the uptake of the intact antibody (11B6) and the lack of uptake of the antibody with an Fc-specific single amino acid point mutation (H435A) in VCaP and LNCaP xenografts. (E) Comparison of heart (blood pool) and prostate with the radiolabeled 11B6 and Fc-binding mutant (H435A) in a genetically engineered mouse model. (F) Ex vivo biodistribution of 11B6 and H435A antibodies in genetically engineered mice at 320 h after injection. Dissected lobes of the prostate were read separately: VP, ventral prostate; AP, anterior prostate; DLP, dorsolateral prostate.

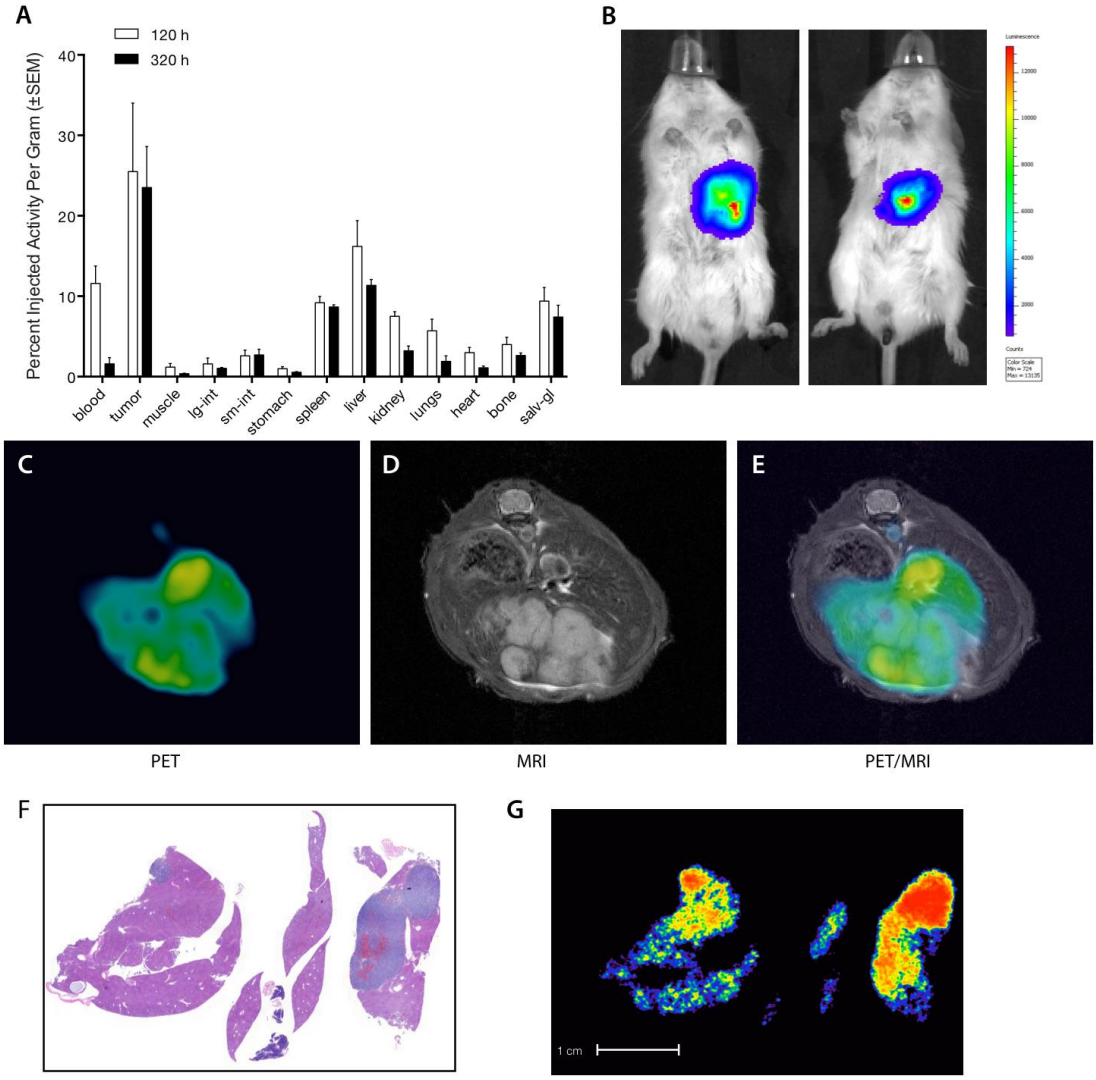

Supplementary Figure 13. Imaging cross-activation of the AR pathway in LREX′ models. (A) Biodistribution of ^{89}Zr-DFO-11B6 in flank xenografts of the enzalutamide-resistant LREX’ model in castrated animals with daily enzalutamide and dexamethasone treatment. We next developed a model of LREX′ liver metastasis by orthotopic implantation of the cells in Matrigel in animals similarly supplemented with dexamethasone and enzalutamide. Metastasis burden was monitored by (B) bioluminescent imaging and (C-E) PET/MR using ^{89}Zr-DFO-11B6. (F, G) H&E and autoradiography of the distribution of the tracer at metastatic deposits within the liver (scale bar is 2 mm).

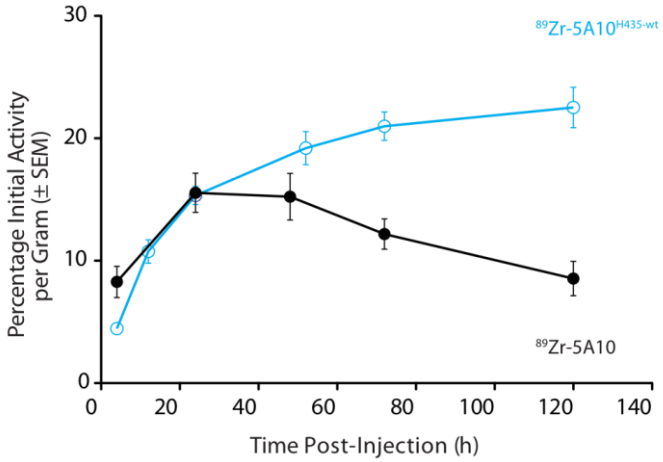

Supplementary Figure 14. Accumulation of reengineered anti-PSA antibody. Radiolabeled ^{89}Zr-antibody uptake in LNCaP flank tumors in nude mice. 5A10, an antibody targeting free PSA, experiences transient uptake in LNCaP xenografts (black, closed circles). When the CDR binding regions were grafted onto the 11B6 antibody scaffold, retaining free PSA specificity (5A10$^{H435\text{-}wt}$), we observed non-transient tumoral accumulation of the antibody (blue, open circles).

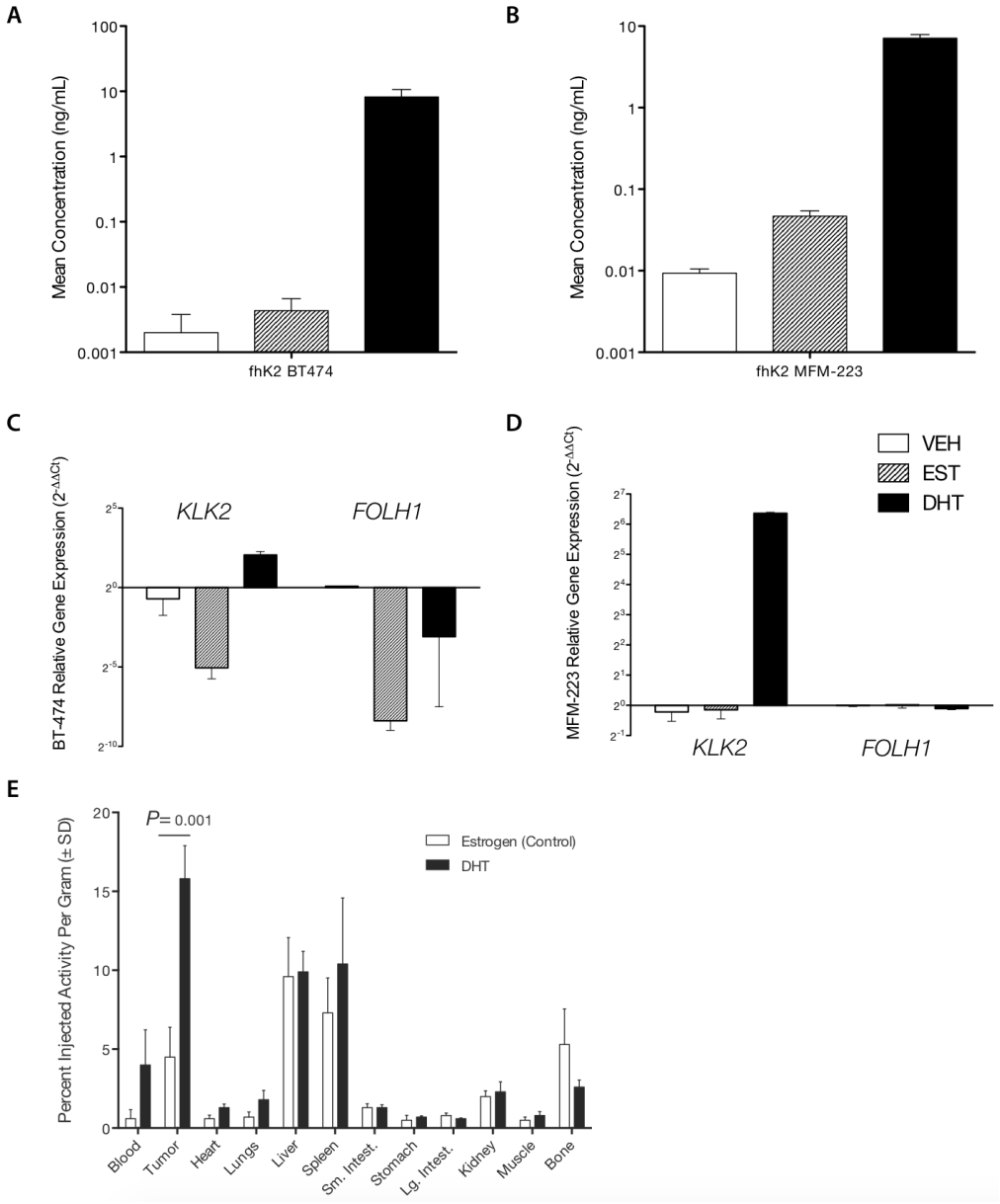

Supplementary Figure 15. hK2 production after DHT stimulation. AR-positive breast cancer cell lines were found to secrete hK2 into the cell culture medium as detected by immunofluorimetric assay after DHT stimulation. The values for free hK2 (fhK2) for the positive cell lines (A) BT-474 and B) MFM-223 are shown here without treatment (vehicle; VEH), with irrelevant hormone addition (estrogen; EST), and with testosterone (DHT). Note that the plots are on a log10 scale. RT-PCR was performed on the cells to compare the expression of *KLK2* and *FOLH1* in (C) BT-474 and D) MFM-223. (E) In vivo biodistribution of ^{89}Zr-11B6 in BT474 xenografts with estrogen and DHT stimulation.

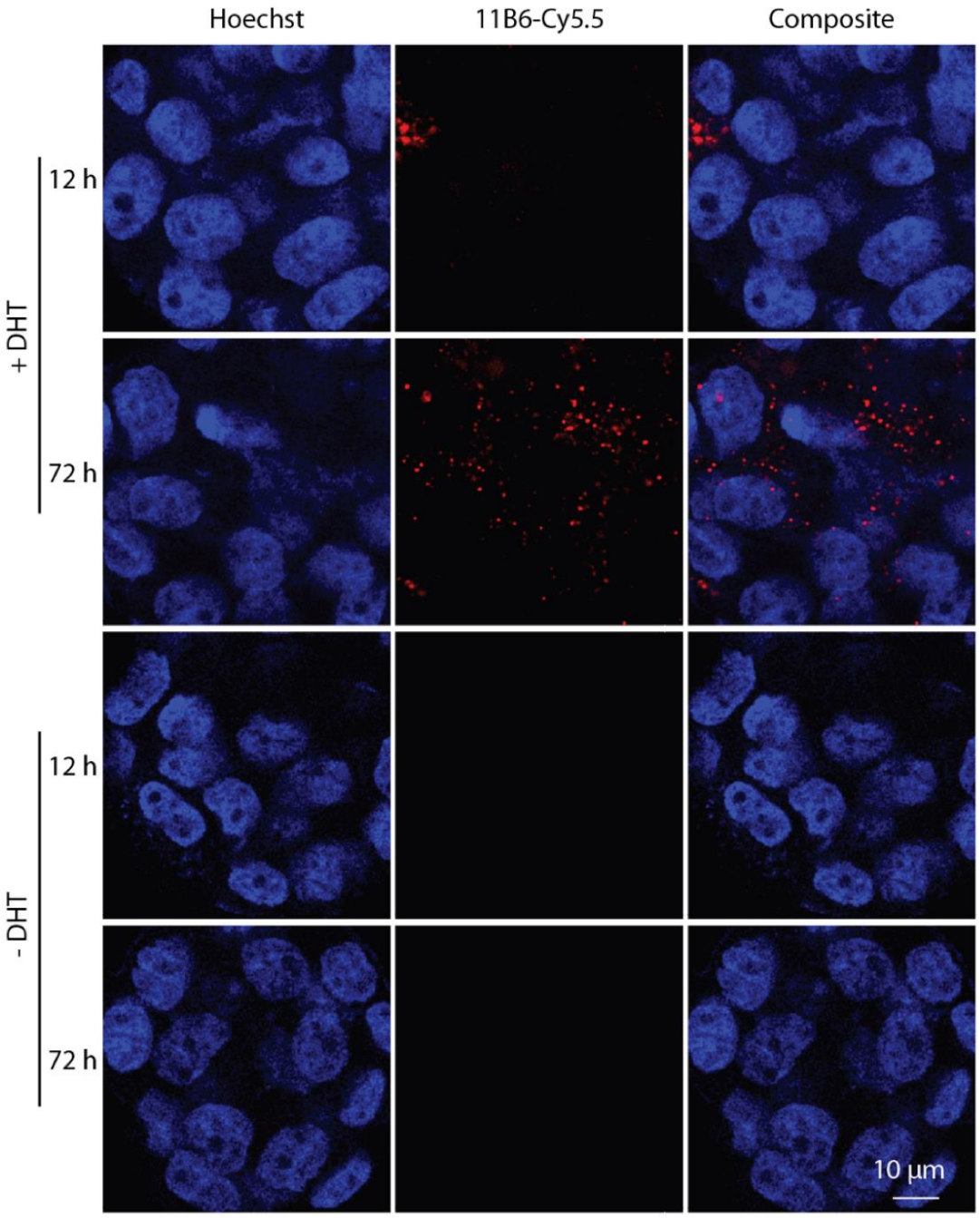

Supplementary Figure 16. Intracellular accumulation of 11B6-hK2 in BCa cells. Under DHT stimulation, the AR-positive BT474 expresses hK2. Conjugated 11B6 is internalized in a time-dependent manner by the stimulated cells. Cy5.5-11B6, red; DAPI, blue.

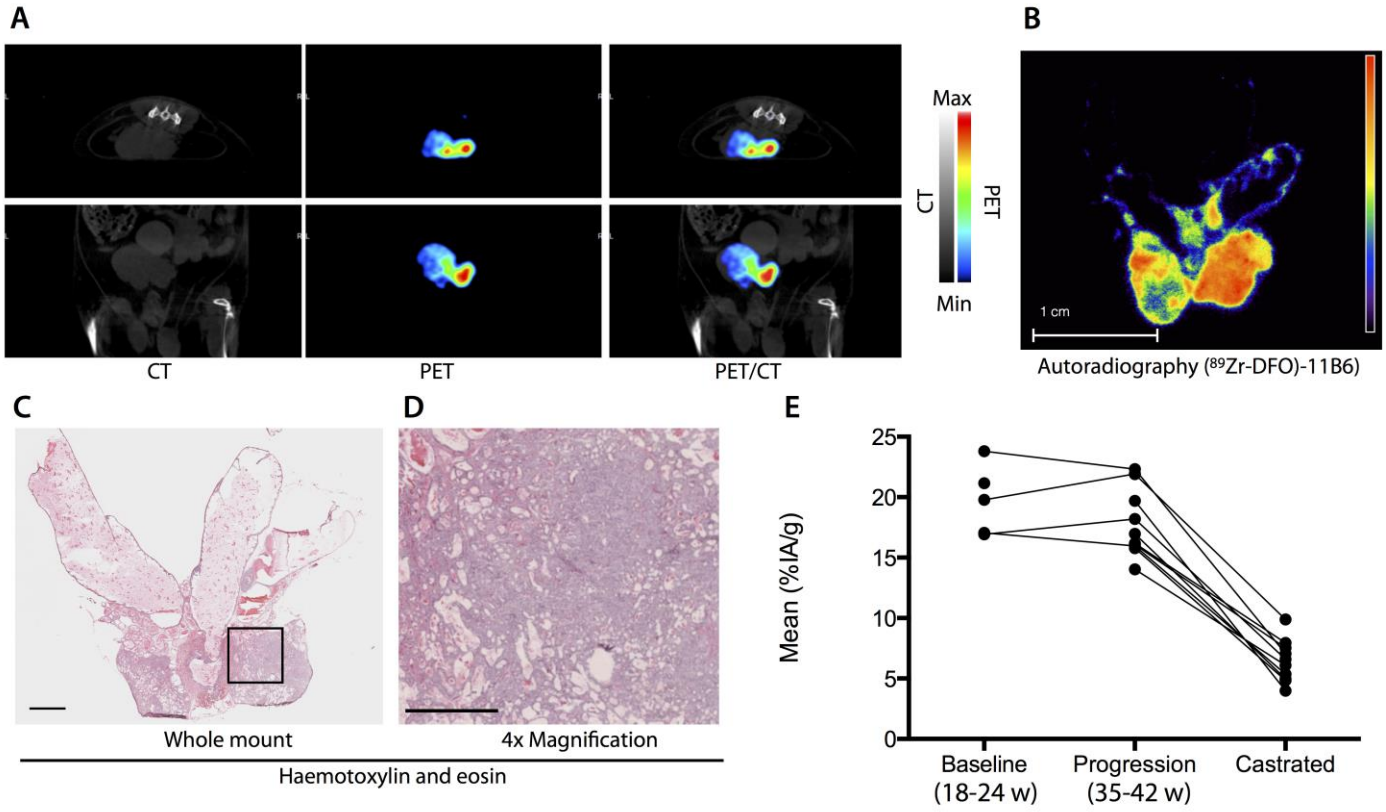

Supplementary Figure 17. Quantitation of ^{89}Zr-11B6 uptake in transgenic PCa mice. (A) Representative CT, PET, and fused PET/CT of 50-week-old mouse. (B) Ex vivo autoradiography (scale, 1 cm) and (C, D) histology confirm prostate and tumor-specific uptake (scale, 250 µm and 100 µm, respectively). (E) ^{89}Zr-DFO-11B6 uptake in the transformed prostate was determined non-invasively by volume of interest measurement at baseline (ages 18–24 weeks), during disease progression (35–42 weeks of age), and after castration. Mean percent injected dose per gram of the prostate as defined on PET imaging.

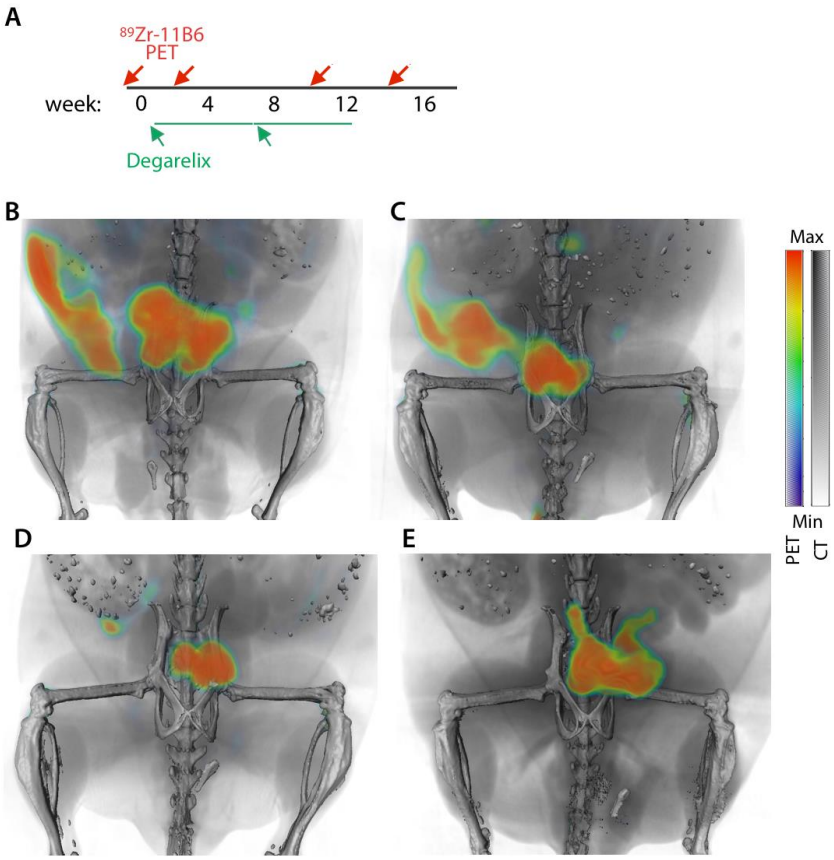

Supplementary Figure 18. Serial PET/CT monitoring ^{89}Zr-11B6 uptake before, during, and after reversible castration by GnRH receptor blockade. (A) Treatment and ^{89}Zr-11B6 PET imaging schedule throughout testosterone-depleting degarelix therapy. (B) Initial PET/CT before treatment (12 weeks of therapy consisting of 2 consecutive depot injections of degarelix acetate). Representative images (C) 2, (D) 10, and (E) 14 weeks after treatment initiation.

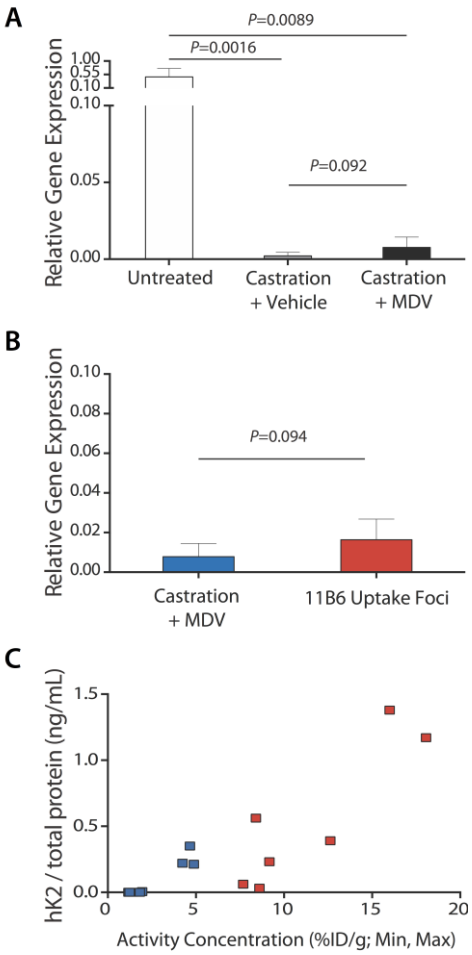

Supplementary Figure 19. Noninvasive monitoring of AR status with ^{89}Zr-DFO-11B6. (A) Relative expression of *KLK2* in prostate tissue collected from Pb_*KLK2 X* Hi-Myc mice without treatment or treated with castration and vehicle (saline) or with castration and adjuvant enzalutamide. (B) PCR analysis of *KLK2* gene expression in tissues treated with castration and enzalutamide resected with ^{89}Zr-DFO-11B6 guidance (red) and prostate tissues negative for 11B6 uptake (blue). (C) Plot of the amount of hK2 protein (normalized to the total protein concentration) in tissues from Pb_*KLK2 X* Hi-Myc mice treated with full androgen blockade correlated with ^{89}Zr-DFO-11B6 uptake minimum (blue) and maximum (red) values.

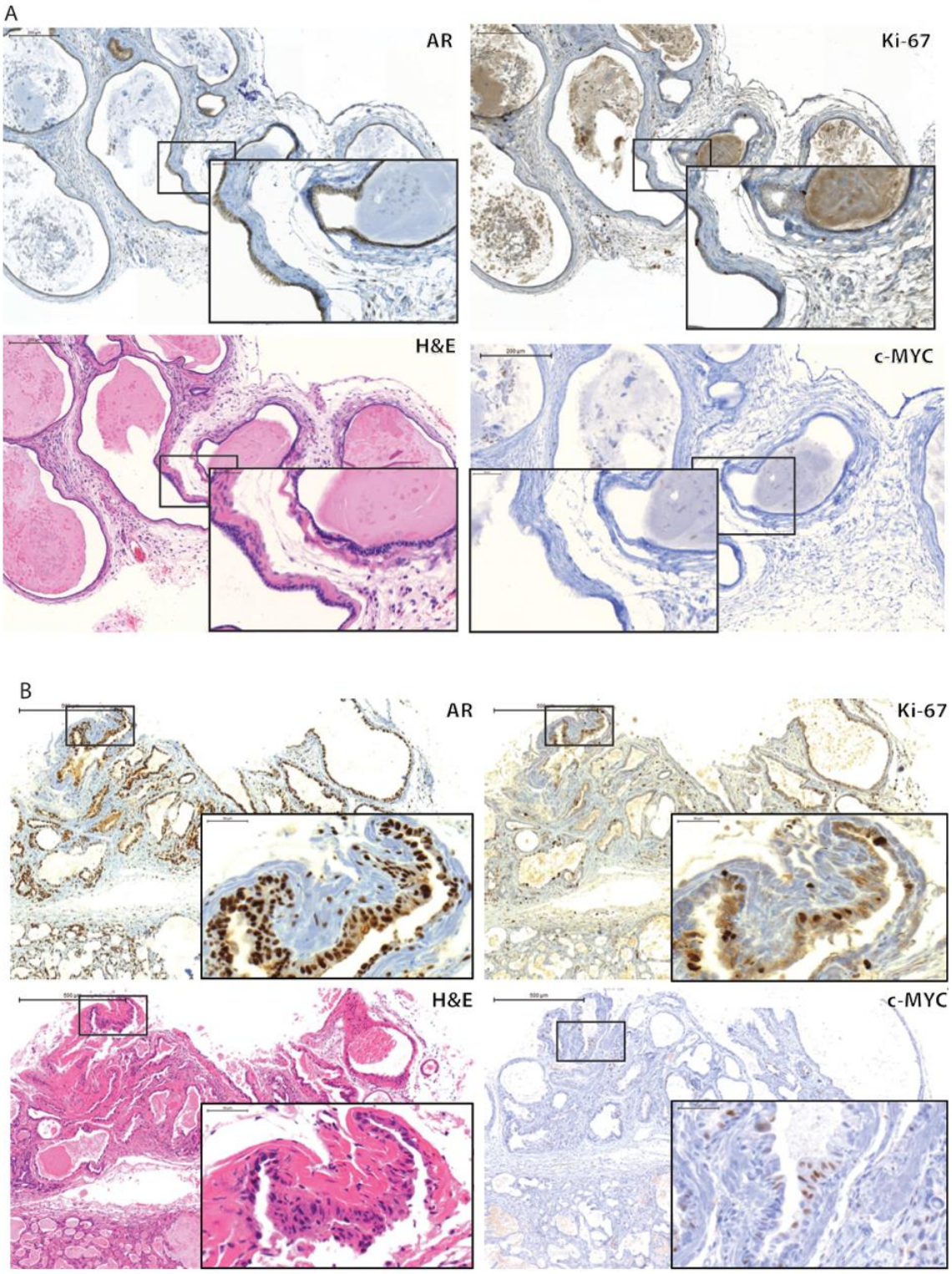

Supplementary Figure 20. Pathological analysis of sections of GEMM of disease after castration. (A) 10 µm sections of tissue that did not demonstrate uptake of 11B6 imaging probe after castration and (B) sections from a 11B6 signal-positive tissue. 10× micrographs (scale bars 500 µm) with 40× insert (scale bars 50 µm). Stain annotated in top right of each micrograph.

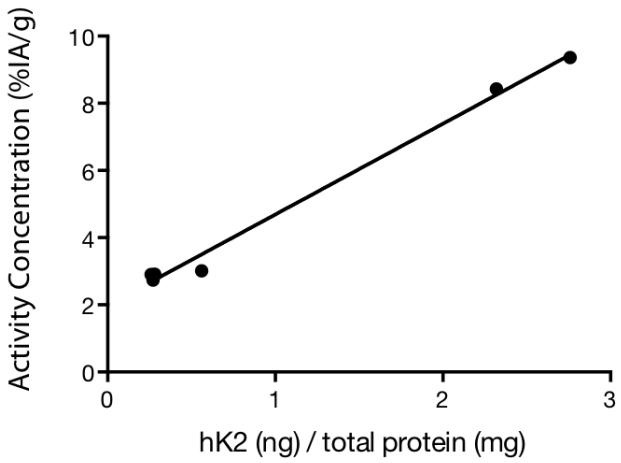

Supplementary Figure 21. Concordance between quantitative ex vivo imaging and protein content. Uptake of ^{89}Zr-DFO-11B6 on PET (measured as %IA/g in volumes of interest from PET imaging) in individual prostate lobes correlated to tissue content of hK2 (normalized to the total protein concentration). R^2 is 0.9928.

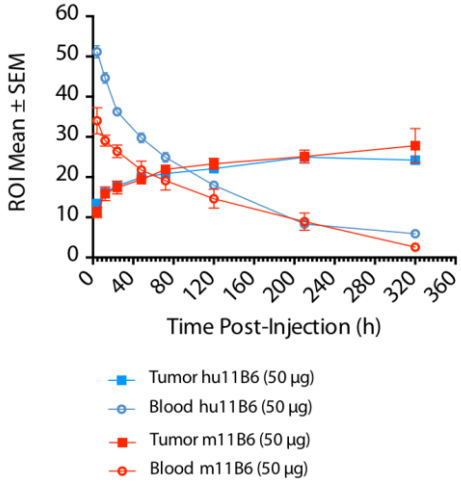

Supplementary Figure 22. Comparison of human and murine 11B6. Humanization of the antibody did not affect the binding and uptake of radiolabeled antibody in xenograft models of prostate cancer (LNCaP; n = 4). Serial microPET images were analyzed for uptake at the tumor site and in the blood (assessed from manually delineated volumes of interest of the xenograft and heart, respectively), and mean volume of interest values are presented as %IA/g.

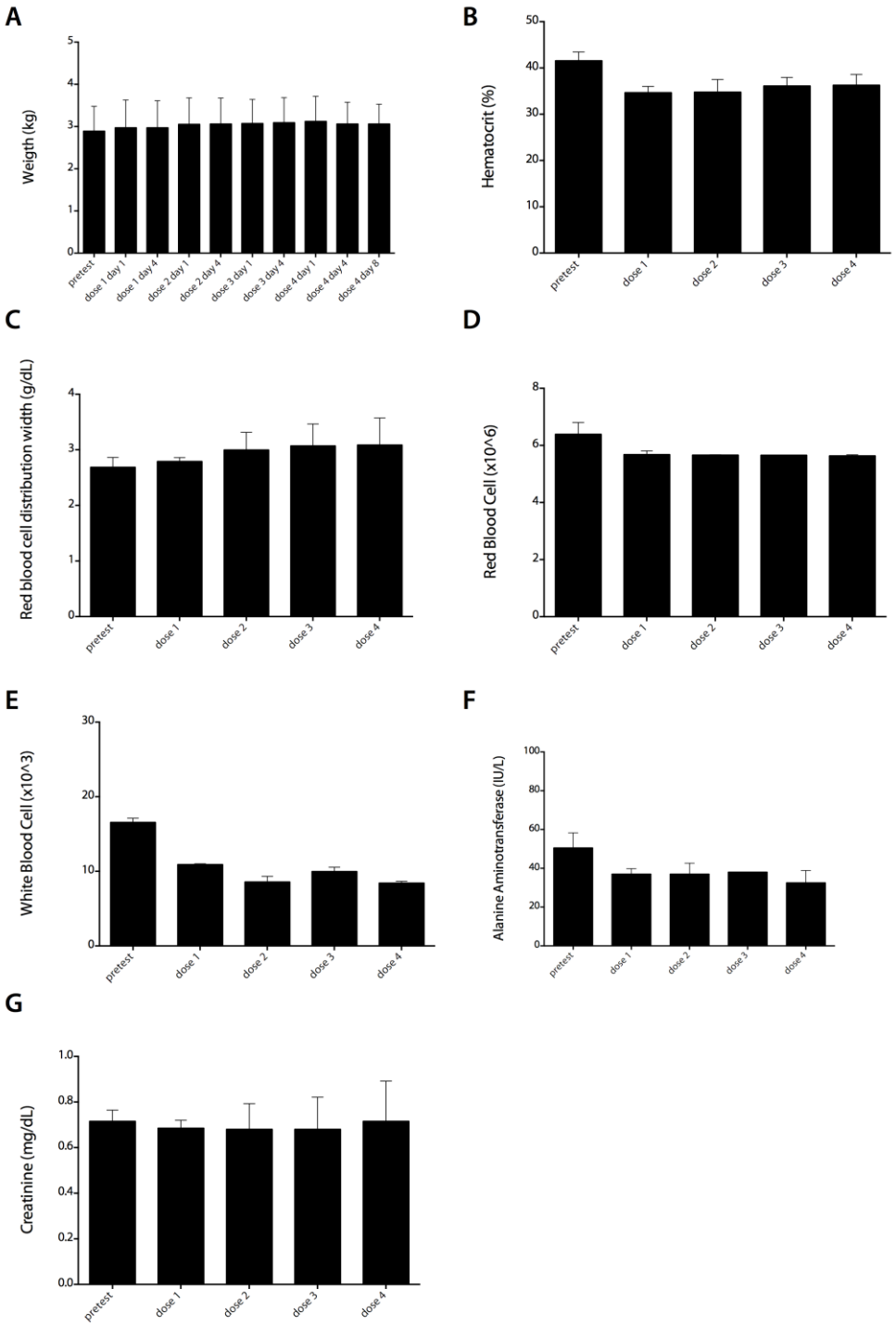

Supplementary Figure 23. h11B6 in cynomolgus monkey. (A) Weight and blood parameters including (B) hematocrit ratio, (C) red blood cell distribution width, (D) red blood cell count, (E) white blood cell count, as well as clinical chemistry values (F) alanine aminotransferase and (G) creatinine after a weekly dose escalation study of humanized 11B6 in male monkeys. These non-human primates express the hK2 protein. No major toxicities were observed, and changes in WBC values may be the result of repeated blood sampling.

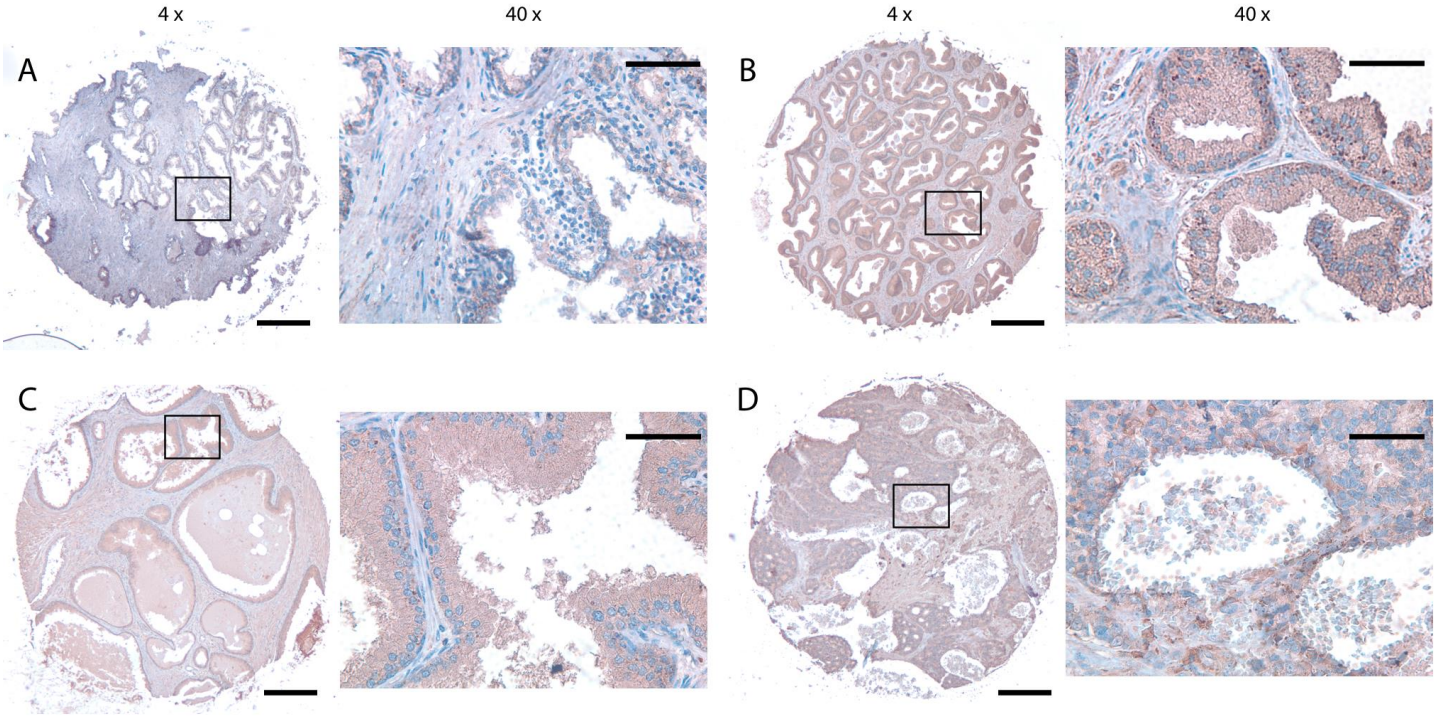

Supplementary Figure 24. h11B6 immunohistochemistry. To evaluate 11B6 binding of kallikrein-related peptidase (free hK2), we applied the murine 11B6 antibody with an anti-rodent secondary antibody to human prostate and prostate cancer biopsy specimens. Hematoxylin counterstained specimens showed the glandular structure of the prostate and hK2 distribution in the prostatic alveoli and intraluminal secretions of representative samples, including (A) the normal prostate, (B, C) two representative prostate tumor tissue specimens, and (D) metastatic foci (lesion in the bone). Scale bars in 4x images are 250 µm, and in 40x inserts they are 50 µm.

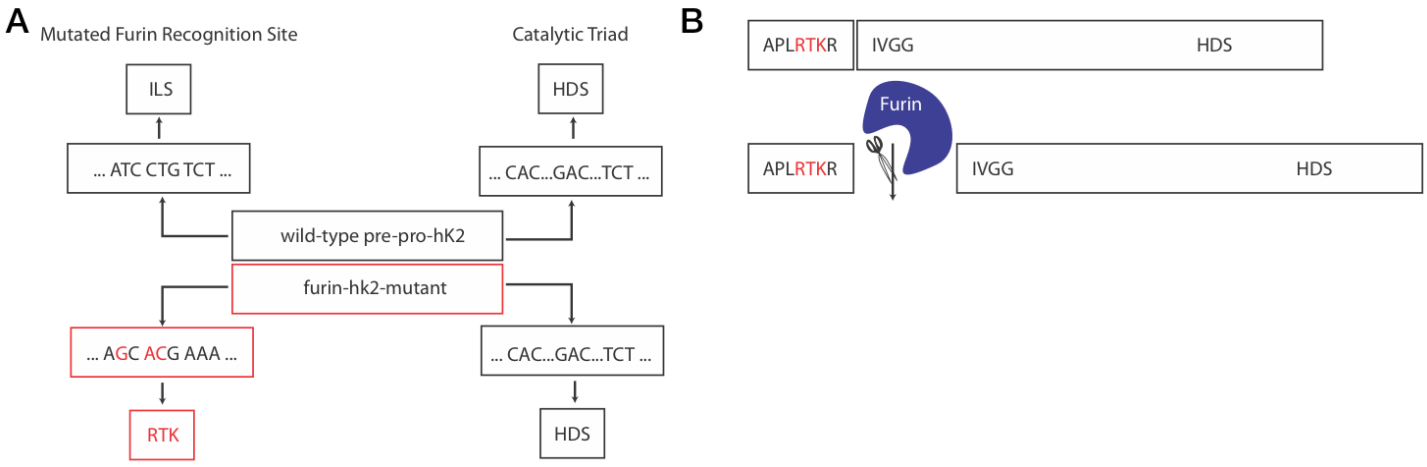

Supplementary Figure 25. Schematic representation of prostate-specific active hK2 in a genetically engineered KLK2-expressing mouse model. (A) Schematic representation of the generation of the Furin protease activated pre-pro-hK2 GEM to yield a prostate-specific, catalytically active hK2 in vivo. Furin cleavage site sequence was inserted upstreatm of the catalytic region of pre-pro-hk2. (B) The Furin protease cleavage site is selectively severed by prostate-specific Furin expression, releasing catalytically active hK2.

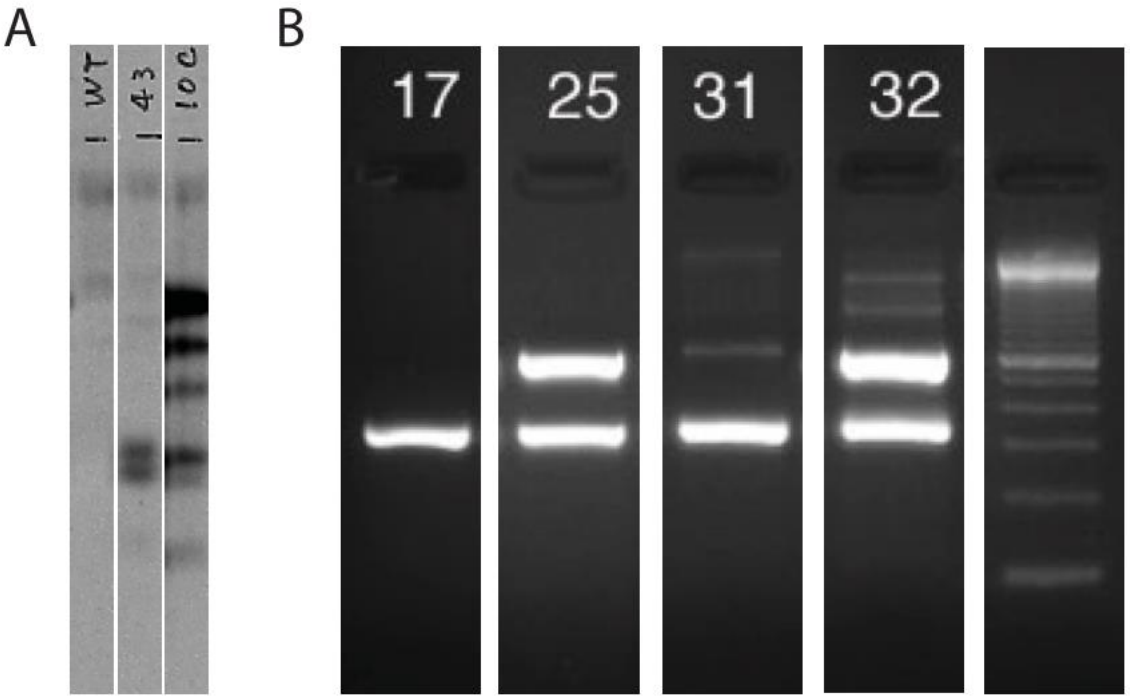

Supplemental Figure 26. Genotyping. (A) Southern blot of BAMHI-digested samples from control (lane annotated WT) and transgenic mice hybridized with a 2.3 Kb Probasin-fur-hK20-SV40 site probe (annotated 43). This positive founder was used for further breeding. The size markers on the right correspond to BAMHI-digested fragments of lambda Hind III, at a dilution corresponding to 10 copies (annotated 10C). (B) PCR evaluation of candidate transgenic and control mice for the incorporation of *FurhK2* cDNA (upper bands); *Gapdh* cDNA (lower bands) indicates equal loading. Lane numbers refer to individual genotyped animals. Sample number 25 correlates to the mouse selected for further breeding (founder line 43). Controls include non-crossed animal (annotated 17), HK2 spiked (31), and Furin-hK2 spiked (32) wild type animals. Invitrogen 100 base pair ladder shown at right.

Supplementary Table 1. Dissociation rate constants (k_{off}) for m11B6, hu11B6, and DFO-conjugated hu11B6. Based on the two measurement series taken for each antibody, no significant difference in the dissociation rate constants (k_{off}) was found between the hK2 targeting antibodies.

Antibody	$k_{off}(10^{-5}s^{-1})Fc2$	$k_{off}(10^{-5}s^{-1})Fc3$	$k_{off}(10^{-5}s^{-1})Fc4$	*Mean*	*Std dev*
m11B6	1.9	4.9	-	3.4	± 2.1
hu11B6	6.4	6.9	-	6.7	± 0.4
hu11B6-DFO	5.8	5.5	-	5.7	± 0.2

Supplementary Table 2. Average association rate constant based on 15 to 18 measurements for each version of 11B6. Differences in rate constants (k_{on}) of the tested antibodies were not significant.

Antibody	*No. of expts fitted*	*Mean* k_{on} $(10^5M^{-1}s^{-1})$	*Std dev*
m11B6	18/18	2.48	± 0.85
hu11B6	15/18	1.17	± 0.38
hu11B6-DFO	18/18	1.11	± 0.22

Supplementary Table 3. Dissociation rate constants (K_d) for the tested antibodies.

Antibody	*Mean K_D 10^{-11} M*	*Std dev*
m11B6	19	± 15
hu11B6	65	± 25
hu11B6-DFO	54	± 13

Supplementary Table 4. ^{89}Zr-11B6 biodistribution and the effect of blocking with cold antibody. Biodistribution values for each organ are shown as percent injected activity per gram at 320 h for different cell lines. Data are shown as mean ±standard deviation with n ≥ 3.

	LNCaP		VCaP		DU145		Blocked (LNCaP)	
Organ	Avg.	±	Avg.	±	Avg.	±	Avg.	±
Blood	3.05	0.61	2.28	1.11	6.48	1.90	4.01	1.25
Tumor	24.72	2.41	80.68	15.34	1.25	0.58	6.42	2.91
Heart	1.60	0.19	0.98	0.20	2.47	0.26	2.46	0.63
Lung	3.60	0.50	2.08	0.37	5.16	0.66	3.81	1.74
Liver	13.80	2.47	11.64	3.97	16.77	1.01	12.82	0.37
Spleen	6.56	2.86	8.58	2.00	4.39	0.33	6.33	1.08
Stomach	0.29	0.10	0.31	0.22	0.86	0.35	0.27	0.08
Sm. Intest.	0.52	0.07	0.48	0.14	3.37	4.45	0.41	0.07
Lg. Intest.	0.42	0.05	0.51	0.17	0.81	0.38	0.36	0.10
Kidneys	4.10	0.08	1.96	0.37	5.00	0.35	4.59	1.23
Muscle	0.38	0.16	0.44	0.12	0.60	0.13	0.57	0.24
Bone	5.52	2.18	1.40	0.56	1.23	0.32	6.33	3.42

Supplementary Table 5. Receptor status of BCa cell lines and secretion of hK2 in response to DHT. The status of estrogen and progesterone receptor and HER2 amplification, as well as the presence of AR for common breast cancer cell lines are given. These 13 BCa cell lines were tested by immunofluorimetric assay for the presence of hK2 protein secretion in culture supernatant. No cells produced the kallikrein without hormone stimulation, and only AR-positive cell lines were found to produce hK2 after the addition of the hormone.

Human breast cancer line	Hormone status				hK2 produced after AR/PR stimulation
	Estrogen receptor	Progesterone receptor	HER2	Androgen receptor	
AU565	–	–	+	–	–
BT-20	–	–	–	–	–
BT-474	+	+	+	+	+
HCC1806	–	–	–	–	–
MCF7	+	+	–	–	–
MDAMB361	+	+	+	–	–
MDAMB415	+	–	–	–	–
MDAMB435	–	–	–	–	–
MDAMB468	–	–	–	–	–
MFM-223	–	–	–	+	+
SK-BR-3	–	–	+	–	–
T-47D	+	+	–	+	+
ZR-75-30	+	–	+	–	–

Supplementary Table 6. Data values from PET, bioluminescence, and clinical chemistry measurements. The data are shown for each group before and after castration, along with average and standard deviation computations. Insufficient volumes of blood for two animals in the PSA assay reduce the group size for this measurement to n = 4.

Measurement (units)	89Zr-11B6 (mean %IA/g)		Average Radiance (p/s/cm2/sr)		Total PSA (ng/mL)		18F-NaF (mean %IA/g)	
	Untreated	Post-Castration	Untreated	Post-Castration	Untreated	Post-Castration	Untreated	Post-Castration
	14.64782	6.861449	10640000	86260		1.1595	7.26063	7.077255
	25.77738	8.707577	11030000	766700	4.0825		6.85531	7.534436
	19.49468	9.22105	5439000	289600	3.841	2.5045	8.851907	10.70157
	13.95731	6.919245	9004800	84100	2.405	3.4995	9.11639	8.213374
	24.19821	7.811357	12136000	345910	10.539	18.9705	7.650328	7.01773
Average:	18.4693	7.9273	9028450	306665	5.216875	6.5335	7.946913	8.108873
SD:	5.3777	1.0542	2608328	278957	3.62452269	8.346592958	0.992123319	1.526253977

Supplementary video 1. Confocal z-stack through prostate gland of genetically engineered hK2-expressing mouse. Internalization and distribution of the fluorophore (cyanine 5.5) labeled 11B6 antibody targeting active-hK2 in the mouse prostate. 4 μm step in Z per frame. Red, actin; blue, nuclei; green, anti-hK2 antibody 11B6.